Received: 4 April 2020 | Revised: 17 February 2021 | Accepted: 10 March 2021

DOI: 10.1111/bre.12563

RESEARCH ARTICLE

Basin Research | IAS EAGE | WILEY

Assessing first-order BQART estimates for ancient source-to-sink mass budget calculations

Björn Nyberg[1] | **William Helland-Hansen**[1] | **Robert Gawthorpe**[1] | **Fabian Tillmans**[1] | **Pål Sandbakken**[2]

[1]Department of Earth Science, University of Bergen, Bergen, Norway

[2]Equinor ASA, Sandsli, Norway

Correspondence
Björn Nyberg, Department of Earth Science, University of Bergen, P.O. Box 7803, 5020 Bergen, Norway.
Email: bjorn.nyberg@uib.no

Present address
Fabian Tillmans and Pål Sandbakken, Equinor ASA, Sandsliveien 90, 5254, Sandsli, Norway

Funding information
Equinor, Grant/Award Number: 810127

Abstract

Constraining the timing and volume of sediment dispersal in an ancient sedimentary system is vital to understand a basin's infill history. One preferred method for a first-order approximation of ancient sediment load estimates, the BQART model, is based on empirical observations of modern river systems relating basin morphology, topography, climate, run-off and bedrock characteristics. Despite the popularity of such methods, a comprehensive assessment on the validity of using modern river observations to measure sediment load on geological timescales is lacking. Here, we investigate the uncertainties, sensitivities and practicalities surrounding the use of modern empirical observations in general and the BQART model in particular, to evaluate ancient sediment river loads. Although catchment area and relief are the least constrained parameters in an ancient sedimentary system, the temperature parameter may have an even more significant impact in the range of predicted sediment load estimates using a BQART approach. The applicability of BQART is most suitable for regional to continental scale source-to-sink systems that are based on robust paleogeographic and paleoclimatic models of cold (<2°C) or warm temperate (>8°C) climates. One further needs to consider the high amplitude discharge events that can dominate the stratigraphic record which are not captured by historical observations of sediment load over a 30-year period. In addition, our limited understanding of bedload material transport and an unknown pristine environment in the Anthropocene reduce the reliability of modern sediment load estimates for the ancient. Mass budget estimates in deep time based on empirical relationships of modern river systems can thus provide first-order estimates within an order of magnitude but need to consider the limitations imposed by extrapolating the modern to the ancient. Here, we present a framework to consider the suitability of the BQART method for ancient source-to-sink mass budget analyses.

KEYWORDS

BQART, deep-time, mass balance, RoBART, sediment load, source-to-sink

Highlights

- Sensitivity and uncertainty analysis of the BQART method for ancient S2S systems
- Area and relief are the least constrained parameters in hinterland reconstruction
- Cooler climates are less reliable in BQART sediment load estimates
- High uncertainty in bedload transport and low-frequency high discharge events

1 | INTRODUCTION

On geological timescales, inferring sediment budgets of ancient source-to-sink (S2S) systems is important to understand the temporal and spatial infill pattern of a basin's history (Allen et al., 2013; Helland-Hansen et al., 2016). One of the main challenges is to reconstruct the conditions of the paleo-drainage that once controlled the generation, transport and deposition of sediment along the routing system. A number of approaches have been developed including surface exposure dating (Covault et al., 2013; von Blanckenburg, 2005), paleo-sediment discharge estimates from empirical methods, such as the BQART model (Syvitski & Milliman, 2007), clinoform progradation dynamics (Petter et al., 2013), scaling relationships (Allen et al., 2013; Nyberg, Helland-Hansen, et al., 2018; Sømme et al., 2009), thermochronological constrained bedrock erosion rates and bulk diffusivity (Allen et al., 2013) and paleohydraulic estimation (Holbrook & Wanas, 2014) techniques, to name a few.

In particular, the BQART model that predicts total suspended sediment load of modern river systems to global oceans has in recent years gained popularity as a first-order estimate for mass budgets in ancient sedimentary systems (e.g., Allen et al., 2013; Blum & Hattier-Womack, 2009; Brewer et al., 2020; Eide et al., 2018; Lin et al., 2018; Liu et al., 2019; Lyster et al., 2020; Sømme et al., 2011, 2013, 2019; Watkins et al., 2018; Zhang et al., 2018). The BQART model expands on the early work of Milliman and Meade (1983) who showed strong scaling relationships between the size of a river system and observed suspended sediment load. By relating a catchment's erodibility (B) including factors of glacial, lithology and anthropogenic impacts, water discharge (Q), area (A), relief (R) and annual temperature (T), the BQART model claims to explain 96% variance in observed long-term (ca. 30 years) total suspended sediment load. The model is calibrated to a global dataset of 488 rivers, spans six orders of magnitude and accounts for 63% of the world's total land surface across a range of climatic and tectonic regions (Syvitski & Milliman, 2007).

The simplicity of the parameters required to define the BQART model is of particular interest in ancient S2S studies considering past hinterland conditions are rarely preserved (Helland-Hansen et al., 2016). In the last decade, methods to define parameters and reduce uncertainty in the BQART model for the ancient have significantly advanced including the use of provenance analysis, morphological scaling relationships and Monte Carlo simulations (e.g., Sømme et al., 2011; Zhang et al., 2018). Improved water discharge estimates can be defined by relating climate zones and runoff to observed sedimentary characteristics (Eide et al., 2018). Additionally, paleogeography and paleoclimate modelling including the use of paleo-digital elevation help constrain geomorphic attributes such as catchment area and relief but also precipitation and water discharge estimates (Lyster et al., 2020).

However, few studies have focused on the sensitivity and uncertainty related to the original BQART methodology and its applicability to the ancient. Helland-Hansen et al. (2016) notes that the approach does not capture the low-frequency, high-amplitude events which may dominate a significant portion of sediment transport and deposition on geological timescales. In addition, the method does not account for bedload material and appears more sensitive to uncertainty in temperature of cooler climates (Lyster et al., 2020). Analytically, catchment area is the largest potential source of uncertainty ranging five orders of magnitude (Eide, Klausen, et al., 2018) and combined with estimation of catchment relief is suggested to be the largest uncertainty in the BQART model for ancient S2S studies (Brewer et al., 2020). Therefore, the BQART method is suggested to be less reliable for application on deep geological time (Brewer et al., 2020).

The aims of this manuscript are to (a) discuss the practical bounds and uncertainty in the original BQART model, (b) investigate the sensitivity of the different parameters, and (c) to evaluate the practicality of the BQART method for ancient S2S mass budget calculations.

2 | BQART PARAMETERS AND CONSTRAINTS

The BQART method of Syvitski and Milliman (2007), determining the total suspended sediment load (Tss) of sediment routing systems, is expressed by:

$$\mathrm{Tss} = \mathrm{wBQ}^{0.31}A^{0.5}\,RT \;\text{for}\; T \geq 2\,^{\circ}\mathrm{C} \tag{1a}$$

$$\mathrm{Tss} = 2\mathrm{wBQ}^{0.31}A^{0.5}R \;\text{for}\; T < 2\,^{\circ}\mathrm{C} \tag{1b}$$

where B is a catchment's erodibility, Q is water discharge in km^3 year^{-1}, A is catchment area in km^2, R is relief in km and T is annual catchment temperature in °C (Figure 1). The w parameter is a constant variable set to 0.02 for Tss in kg/s or 0.0006 for values in MT year^{-1}.

The aim of this section is to introduce the uncertainty and limitations in defining each parameter for use in ancient S2S mass budget evaluations.

2.1 | Catchment erodibility (B)

Catchment erodibility is incorporated within the BQART formula by the B parameter that is explained by the equation:

$$B = \mathrm{IL}\left(1 - T_E\right) E_h \tag{2}$$

where I is glacial erosion, L is lithology, T_E is sediment retention behind dams and E_h is human induced soil erosion.

Given human impact on ancient sedimentary systems does not exist, variables T_E and E_h are removed for ancient S2S analyses. Within the glacial erosion variable, I, erosion is suggested to vary linearly with increasing proportion of glacial coverage within the drainage region by the equation:

$$I = \left(1 + 0.09A_g\right) \tag{3}$$

where A_g ranges from a value of 0–10 representing a glacial coverage between 0% and 100%, respectively.

However, the BQART approach is not suitable for capturing paraglacial and periglacial processes, flash flooding events or different modes of glacial transport (Syvitski & Milliman, 2007). Since the impact of glacial erosion on sediment load can be significant yet remains poorly constrained (e.g., Cook et al., 2020) and the BQART method is defined for an interglacial period, it is best to reserve the method for mass budget analyses with no significant glacial activity.

The remaining catchment averaged lithology parameter (L) is defined based on the descriptions in Table 1 ranging from a value of 0.5–3. Syvitski and Milliman (2007) originally calibrated the L parameter based on the aerial coverage of lithologies within modern river catchments as defined by the global lithology database of Dürr et al. (2005). This L parameter range is consistent with other studies showing the erodibility of landscapes between 0.1 and 7 (Howard, 1994; Restrepo et al., 2015) but reflects average catchment erodibility estimates observed on the global scale. In ancient S2S analyses, provenance and mineralogy studies can help to constrain the likely hinterland lithology and the same descriptions as in Table 1 can be applied to derive a lithology value (e.g., Sømme et al., 2013). However, it is important to consider that the average catchment erodibility factor is an estimate that is not a physical measurement proportional to the distribution of lithologies within a drainage area. For

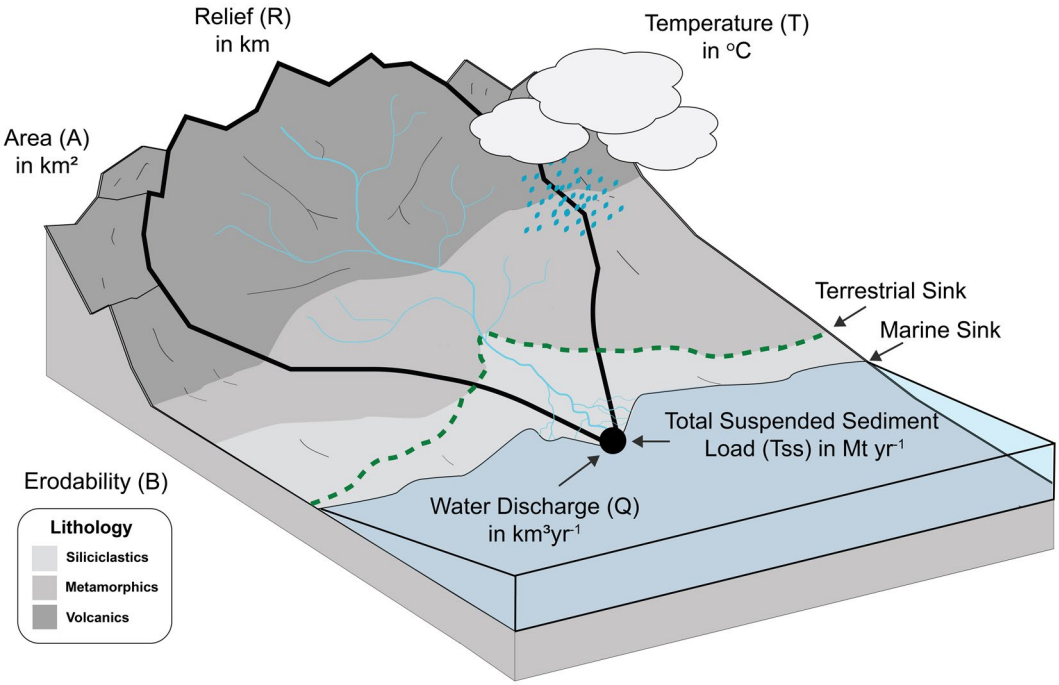

FIGURE 1 Erodibility (B), water discharge (Q), catchment area (A), maximum relief (R) and temperature (T) define parameters in the calculation of total suspended sediment load to oceans using the BQART formula. Modified after Nyberg, Helland-Hansen, et al. (2018) [Colour figure can be viewed at wileyonlinelibrary.com]

example, Figure 1, shows three different lithologies of siliciclastics ($L = 2$), metamorphics ($L = 0.5$) and volcanics ($L = 1$) but its average catchment lithology parameter, L, may be skewed towards only one region associated with higher relief and/or precipitation.

Hence, the average catchment lithology parameter (L) used to calibrate the original catchment dataset in the empirical BQART model does not directly correlate to the aerial extent of different lithologies observed within the drainage region (Cohen et al., 2013; Restrepo et al., 2015). The ternary diagram of Figure 2 shows the lithological composition of the world's largest river catchments by aerial extent categorized into metamorphic/hard rocks, clastic sediments and volcanic/carbonate lithology end-members. Superimposed on Figure 2 are the colour-coded L parameter value (0.5–3) assigned in the original BQART model by Syvitski and Milliman (2007). While there are clear trends between the coverage of lithology in a catchment and the assigned L parameter, one should bear in mind that it is a qualitative description (as defined in Table 1) and not a quantitative physical parameter.

TABLE 1 Description of averaged catchment lithology (L) parameter by Syvitski and Milliman (2007)

B factor	Description
0.5	Acid plutonic and/or high-grade metamorphic rocks
0.75	Hard grade lithologies but mixed
1	Mixed lithologies or carbonates/volcanics
1.5	Softer-mixed lithologies
2	Clastic sediments
3	Loess

The ambiguity in the quantitative thresholds that define a catchment's average erodibility increases uncertainty in the L parameter that needs to be considered in the extrapolation to ancient S2S systems. In addition, vegetation profoundly influences transport of sediment and has changed over geological time (Gibling & Davies, 2012) which is not considered in the catchment erodibility parameter. Given the uncertainty associated with the numerical value attributed to the L factor, it is necessary at the very least to include a twofold uncertainty range (e.g. 0.5–1 or 1–2) based on the variability that is observed from the modern (Figure 2).

Alternatively, a catchments erodibility may be set to the global observed mean of 1 (e.g., Brewer et al., 2020; Lyster et al., 2020; Watkins et al., 2018) which will explain 66% of Tss load using the BQART equation (Syvitski & Milliman, 2007). Based on the original M&S92+ validation database of Syvitski and Milliman (2007), the variance may slightly improve to 70% if correcting for glacial (I) and anthropogenic (T_E and E_h) factors in Equation (2), factors that should not be considered in an ancient S2S study using BQART. Nonetheless, using a B parameter equal to 1 would require a correction for 30%–34% variance in predicted Tss load that is not explained in the BQART equation. Likely, a lithology factor can be constrained to a certain degree within a threefold range by further provenance analysis to distinguish between soft lithologies (erodibility 1–3) or harder

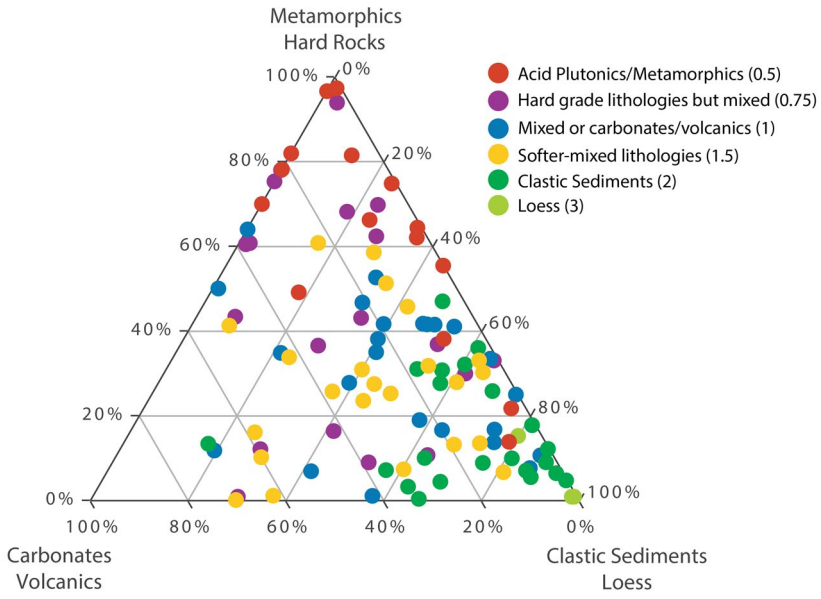

FIGURE 2 Modern river catchments classified by the aerial extent of each catchment's lithology. The ternary diagram, based on Dürr et al. (2005), is used to calibrate the original BQART model. Superimposed on the ternary diagram are colors to indicate the lithology (L) factor (0.5–3) assigned to each catchment as defined by Syvitski and Milliman (2007). Note that the assigned lithology (L) factor loosely correlates to the actual distribution in lithologies within a catchment. The largest 25 catchments in each lithology (L) category are shown except for the Loess lithology that number 4 [Colour figure can be viewed at wileyonlinelibrary.com]

lithologies (0.5–1) which will maintain the claimed 96% variance in the BQART equation.

2.2 | Catchment area (*A*)

Several approaches have been suggested to reconstruct catchment area including scaling relationships (Bhattacharya et al., 2016; Nyberg, Helland-Hansen, et al., 2018; Sømme et al., 2009), paleogeographic reconstructions and provenance analysis (Blum et al., 2017).

Hack's law is an empirical relationship showing that the length of a catchment's river strongly correlates with its catchment area (Hack, 1957; Figure 3a). Subsequent work indicates that the exponent variable of this power-law relationship (a value of 0.6 to calculate river length in miles) may vary slightly (Rigon et al., 1996) but remains valid on regional and global S2S scales (Nyberg, Gawthorpe, et al., 2018; Sømme et al., 2009). However, measuring the length of an ancient river system is difficult even if attempting to correct for a rivers apparent sinuosity. Alternatively, the length of a catchment measured from the river outlet to its drainage divide provides a more practical solution to estimate catchment area (Sømme et al., 2013). Global based regressions, based on the global S2S database of Nyberg, Helland-Hansen, et al. (2018), show a high degree of variability in correlation to catchment area suggesting the method provides at best, a first-order estimate (Figure 3b). Similarly, while the regular spacing of river outlets show constraints on the possible catchment area (Hovius, 1996; Sømme et al., 2013), sedimentary basin and source region geometry vary significantly between systems of different sedimentological and tectonic histories (Nyberg, Gawthorpe, et al., 2018).

Paleogeographic reconstructions provide a better alternative for constraining catchment area that may additionally be supported by provenance analyses including detrital zircons (Blum et al., 2017; Dickinson & Gehrels, 2008). Furthermore, if the paleogeographic reconstructions are constrained by paleo- digital elevation models (paleoDEM; e.g., Markwick & Valdes, 2004; Scotese & Wright, 2018), hydrological tools standard in Geographical Information Systems (GIS) can delineate drainage regions. It is important to note that paleoDEMs are most suitable for regional to continental scale analyses and should contain a degree of uncertainty to account for uncertainty in reconstructing the digital paleogeography and paleotopography maps (e.g., Lyster et al., 2020).

2.3 | Water discharge (*Q*)

Syvitski and Milliman (2007) estimate a rivers water discharge based on a power-law relationship by the equation:

$$Q = kA^m \tag{4}$$

where Q is water discharge in m^3/s, A is catchment area in km^2, k constant equal to 0.075 and a m exponent of 0.8.

Subsequent work by Eide, Klausen, et al. (2018) has shown that, the constant and exponent variables of that power law relationship (k and m, respectively) change based on different run-off (Ro) ranges for different climate zones (Table 2). In fact, the power-law relationship can be removed entirely since the original Milliman and Farnsworth (2011) dataset that Eide, Klausen, et al. (2018) base their assumption, define the hydrological run-off (ro) as a function of water discharge over catchment area. Estimated water discharge can then be simplified by:

$$Q = RoA \tag{5}$$

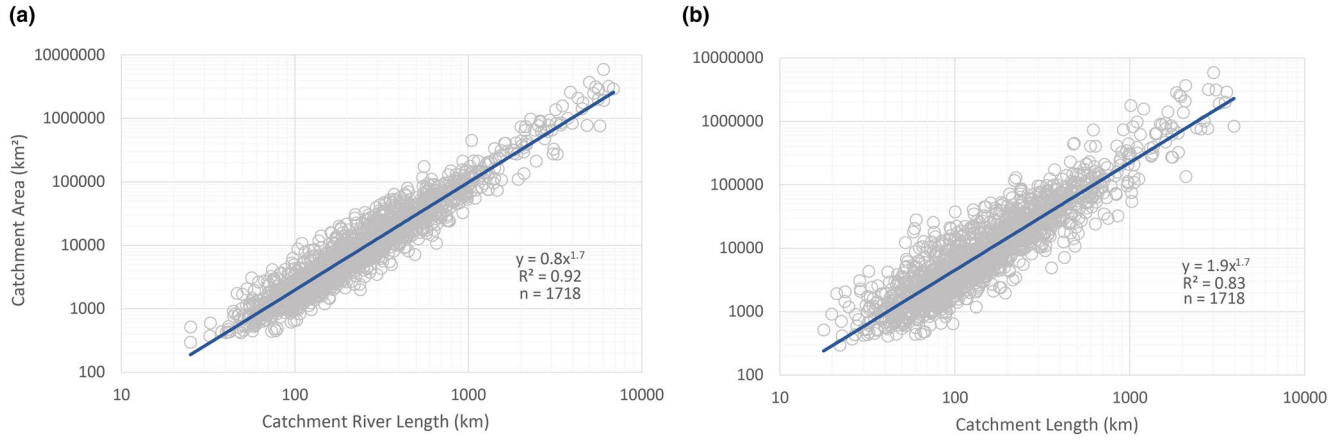

FIGURE 3 (a) Relationship between catchment river length and catchment area following Hack's Law (Hack, 1957). (b) Relationship between catchment length and catchment area. In the application to the ancient, catchment length is easier to derive based on the reconstruction of likely paleo-drainage divide, but has a significantly lower correlation. Data show 1718 modern river catchments with a Tss >1 MT $year^{-1}$ based on the from the Global Source-to-Sink database (Nyberg, Helland-Hansen, et al., 2018) [Colour figure can be viewed at wileyonlinelibrary.com]

TABLE 2 Different equations for calculating water discharge compared to 1,255 observed river systems of Milliman and Farnsworth (2011)

Model	Class	Run-off (mm/year km^{-1})	k	m	r^2
Equation (4) Syvitski and Milliman (2007)	All data	>0	0.075	0.8	0.5
	Non-arid	>100	0.075	0.8	0.74
Equation (4) Eide, Müller, et al. (2018)	All Data	>0	Variable	Variable	0.90
	Arid	0–100	0.0005	1.0633	0.72
	Semi-arid	100–250	0.0063	0.9824	0.98
	Humid	250–750	0.0161	0.9839	0.96
	Wet	750–7,476[a]	0.0873	0.9164	0.99
Equation (5)	All data	>0	N/A	N/A	1

[a]Based on the highest observed runoff value in the Milliman and Farnsworth (2011) database.

where Q is water discharge in km^3 year^{-1}, Ro is run-off in mm/km year^{-1}, and A is catchment area in $10^6 \times$ km^2.

To define the absolute run-off (Ro) values for a paleo-environment is challenging. As originally suggested by Milliman and Farnsworth (2011), a range of run-off values that characterizes different climate zones should rather be used to capture the variability in water discharge for different catchment sizes (e.g., arid—<100, semi-arid 100–250, wet—250–750 and humid 750 > mm km/year). Eide, Klausen, et al. (2018) discussed observations in stratigraphy that may be used to define climate zones and associated run-off values based on paleosols, root types, mineralogy and sedimentary architecture. The advantage of using Equation (5) is that the full possible range in water discharge for each climate zone is captured as opposed to a single averaged value (Table 2). Alternatively, paleoclimate modelling (e.g., Armstrong et al., 2016; Jacob et al., 2001; Sellwood & Valdes, 2008) can provide a useful tool to reconstruct the catchment-wide climate conditions, including precipitation, to define paleo-water discharge for the Q parameter as demonstrated recently by Lyster et al. (2020).

2.4 | Relief (R)

Defining relief of an eroded hinterland is problematic. Nyberg, Helland-Hansen, et al. (2018) concluded that geomorphic scaling relationships of global modern river catchment areas do not correlate with relief given the individuality of each basin undergoing specific tectonic and sedimentological histories. One approach to constrain the likely range of expected relief values is to use modern analogues, grouped by catchment-sizes and its dominant tectonic regime, as a reference (Figure 4). If additional tectonic and sedimentological characteristics of a particular ancient S2S study can filter the analogues used in the Global Source-to-Sink database, the distributions shown in Figure 4 may further be refined (Nyberg, Gawthorpe, et al., 2018). Alternatively, paleoDEMs that define catchment area (e.g., Lyster et al., 2020; Markwick & Valdes, 2004; Scotese & Wright, 2018), if available, may also be used to extract the maximum relief within each delineated drainage region. Other options such as stable isotope-based paleoaltimetry reconstructions (Rowley & Garzione, 2007) and thermochronology exhumation rates (Reiners, 2007) may provide additional reasoning to constrain the R parameter.

2.5 | Temperature (T)

An estimate of paleoclimate can be derived based on a number of proxies including observed terrestrial and marine biomes of flora and fauna, sedimentological analysis of paleosols, coals, mineralogy, river architecture and eolian/evaporite deposits, and stable isotope ratios in marine shells and ice (Eide, Müller, et al., 2018; Sellwood & Valdes, 2008) to name a few. The proxies combined with plate tectonic reconstructions on the distribution of land-water provide the basis for coupled oceanic-atmospheric paleoclimate models (e.g., Jacob et al., 2001; Markwick & Valdes, 2004; Sellwood & Valdes, 2008). It is important that the temperature (T) parameter estimate is an average of the entire drainage region including the preserved terrestrial sink and source region (Figure 1). Finally, the accuracy of the paleo-climate model needs to be taken into consideration including spatial variability within the drainage region as a standard deviation around the mean.

3 | IMPLEMENTATION AND SENSITIVITY

In this section, we will consider the approach to apply the BQART method, the sensitivity and practical bounds of each parameter, and the influence of Monte Carlo simulations

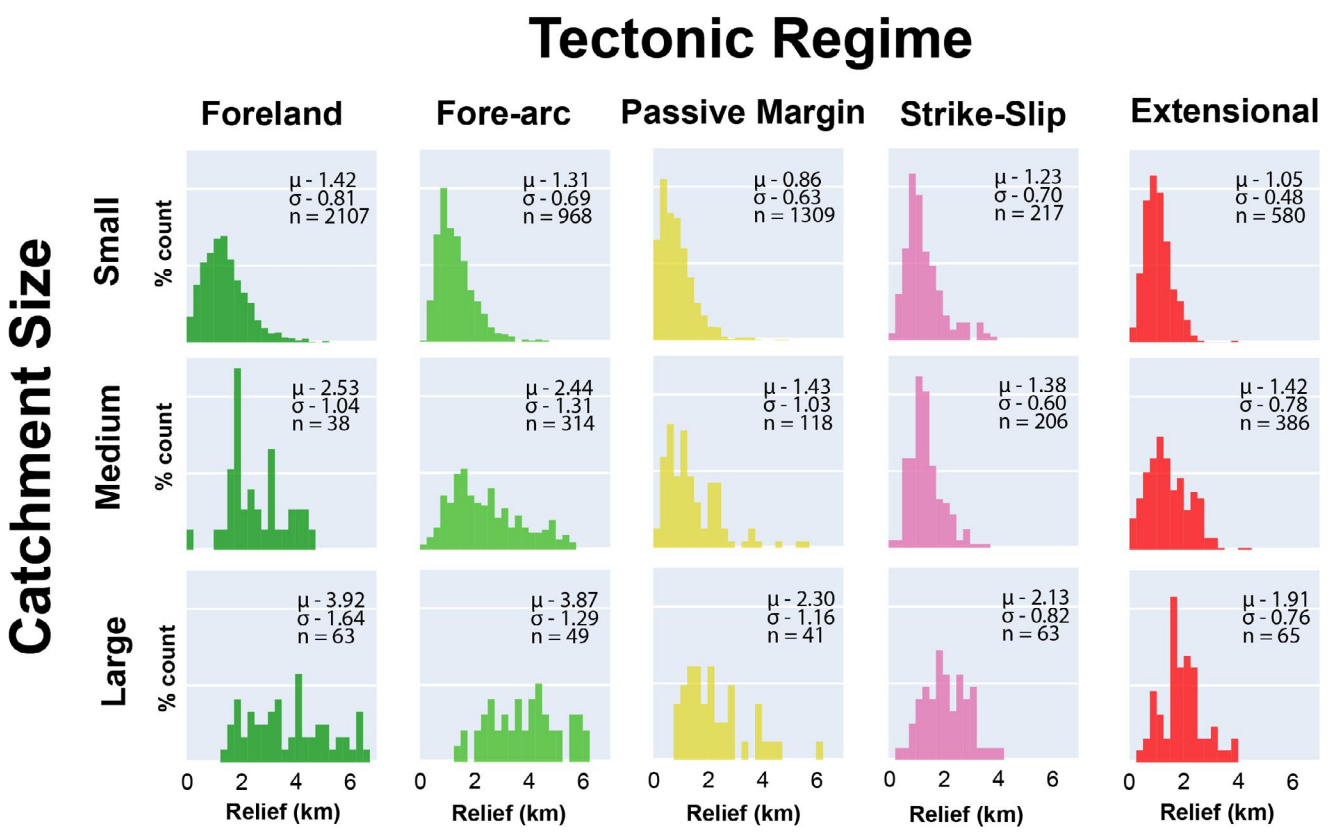

FIGURE 4 Observed distributions in relief by main tectonic regime and either a small (<10,000 km^2), medium (10,000–100,000 km^2) or large (>100,000 km^2) catchment size based on the Global Source-to-Sink database (Nyberg, Gawthorpe, et al., 2018) with a Tss >0.1 MT year^{-1} [Colour figure can be viewed at wileyonlinelibrary.com]

in constraining mass budget estimates for an ancient S2S system.

3.1 | Revised BQART model

The improved water discharge calculation can simplify the original BQART model to a RoBART formula (Equation 6). In this case the total suspended sediment load (*T*ss) is given by:

$$Tss = wRo^{0.31}\mathrm{BA}^{0.81}\mathrm{RT} \text{ for } T \geq 2\,^{\circ}\mathrm{C} \quad (6a)$$

$$Tss = 2wRo^{0.31}\mathrm{BA}^{0.81}R \text{ for } T < 2\,^{\circ}\mathrm{C} \quad (6b)$$

where *Ro* is run-off in mm/km year^{-1}, *B* is catchment averaged lithology based on Table 1, *A* is catchment area in km^2 × 10^3, *R* is relief in km, *T* is annual catchment temperature in degrees Celsius and w is a constant equal to 0.00223 for total suspended sediment load (Tss) in MT year^{-1} (Figure 5).

Equation (6) is derived by analysing the trend between multiple linear regression lines produced by implementing to the BQART formula, the improved water discharge (*Q*) calculation in Equation (5) for different run-off values and catchment sizes (Figure 6). Analytically, the RoBART formula is the exact same equation as the original BQART formula but simply incorporates improved water discharge scaling. The RoBART model in Equation (6) places a slightly higher weight to the catchment area (*A*) parameter with an exponent value of 0.81 compared to the original 0.5 value in Equation (1) by eliminating the redundant *A* parameter used to calculate both water discharge (Equation 4) and Tss load.

The accuracy of the RoBART model (Equation 6), plotted against the observational M&S92+ database (Syvitski & Milliman, 2007) used to calibrate the original BQART formula, is shown in Figure 5. While the coefficient of variance (R^2) for the RoBART method is lower and captures only 84% of the variance compared to the claimed 96% of the BQART model, the linear regression line is skewed towards the higher sediment load values (>1,000 MT year^{-1}). If analyzing the number of catchments within a twofold range of observed Tss load measurements, then the RoBART formula predicts 83% of all river catchments compared to 69% for the original BQART approach. Grid-based numerical implementation of the BQART model by Cohen et al. (2013) that also incorporates improved daily water discharge calculations for the *Q* parameter, show Tss load predictions within a 97% variance.

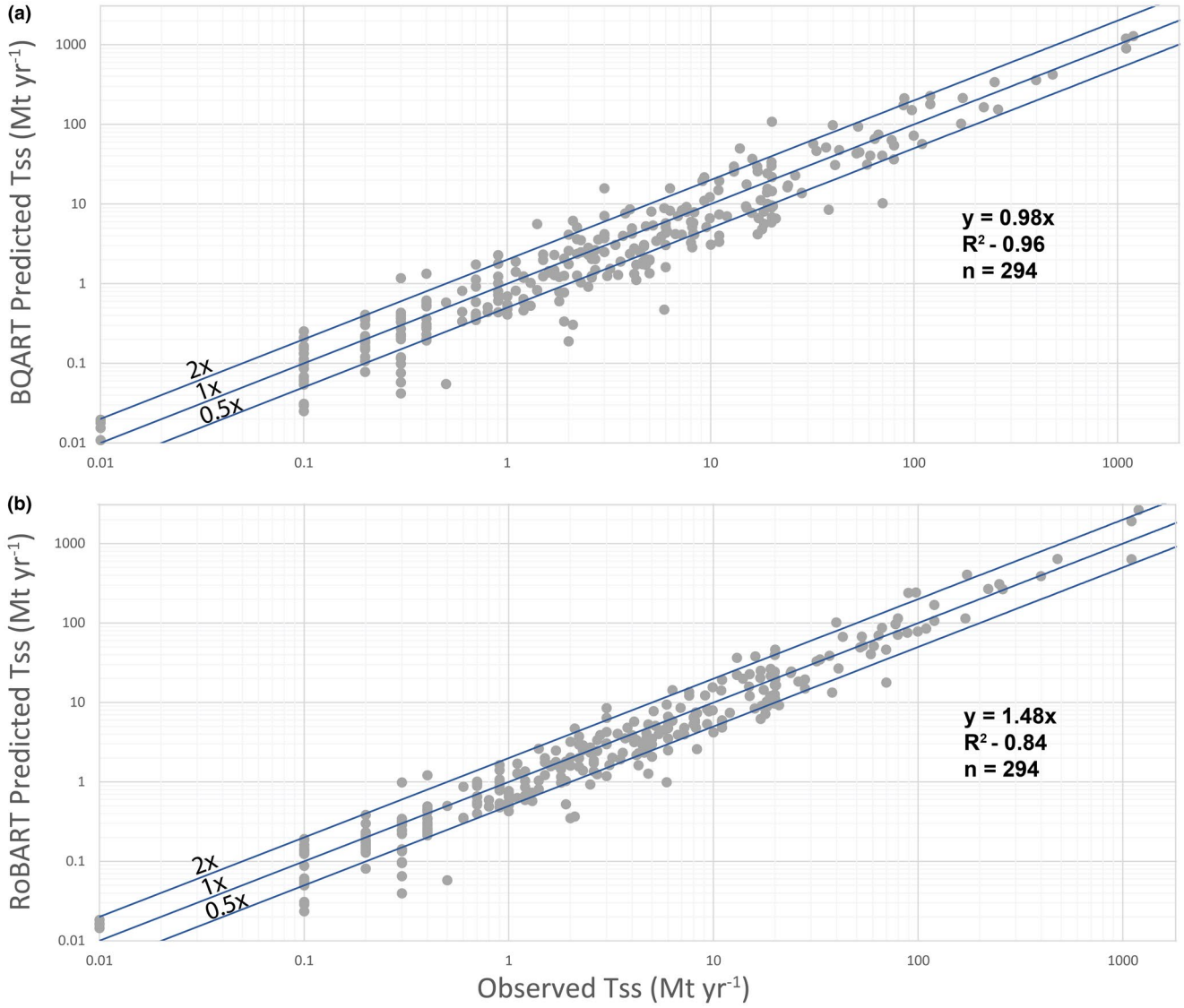

FIGURE 5 Predicted values in Tss load by: (a) the BQART method, and (b) the RoBART method, against the observational M&S92+ database (Syvitski & Milliman, 2007). Overlain on each figure are 1:1, 1:2 and 1:0.5 ratio lines between observed and predicted values [Colour figure can be viewed at wileyonlinelibrary.com]

Hence, we are confident that the simplified RoBART incorporating a better water discharge scaling improves the overall prediction of Tss load estimates. One should also note that while the M&S92+ database is one of the best global databases of long-term (ca. 30 years) modern river observations, there will inherently be errors associated with compilation of data from different sources (Cohen et al., 2013).

3.2 | Sensitivity and practical bounds

The uncertainty in predicted Tss load based on the RoBART (or BQART) calculation will depend on the sensitivity of each parameter and the accuracy in defining each value for ancient source-to-sink systems. For run-off (*Ro*) and catchment area (*A*), the sensitivity on the calculation is explained by the power-law relationships of $Ro^{0.31}$ and $A^{0.81}$ in Equation (6). The lower exponent variable for run-off shows that the parameter is less sensitive in comparison to catchment area. Consequently, a 10-fold range in uncertainty for run-off would yield a twofold range in calculated Tss load, whereas a 10-fold range in uncertainty for catchment area would yield a 6.5-fold range in calculated Tss load. Furthermore, by relating run-off values to different climate zones, the sensitivity is reduced within a 1.3- and 2-fold range (Table 2). In comparison, catchment area spans five orders of magnitude and thus represents a significant source of potential uncertainty (Brewer et al., 2020; Eide, Müller, et al., 2018), although provenance analysis could significantly improve estimates as discussed in Section 2.2.

Catchment erodibility (*B*), relief (*R*) and temperature (*T*) will all scale linearly from the power-law relationship of

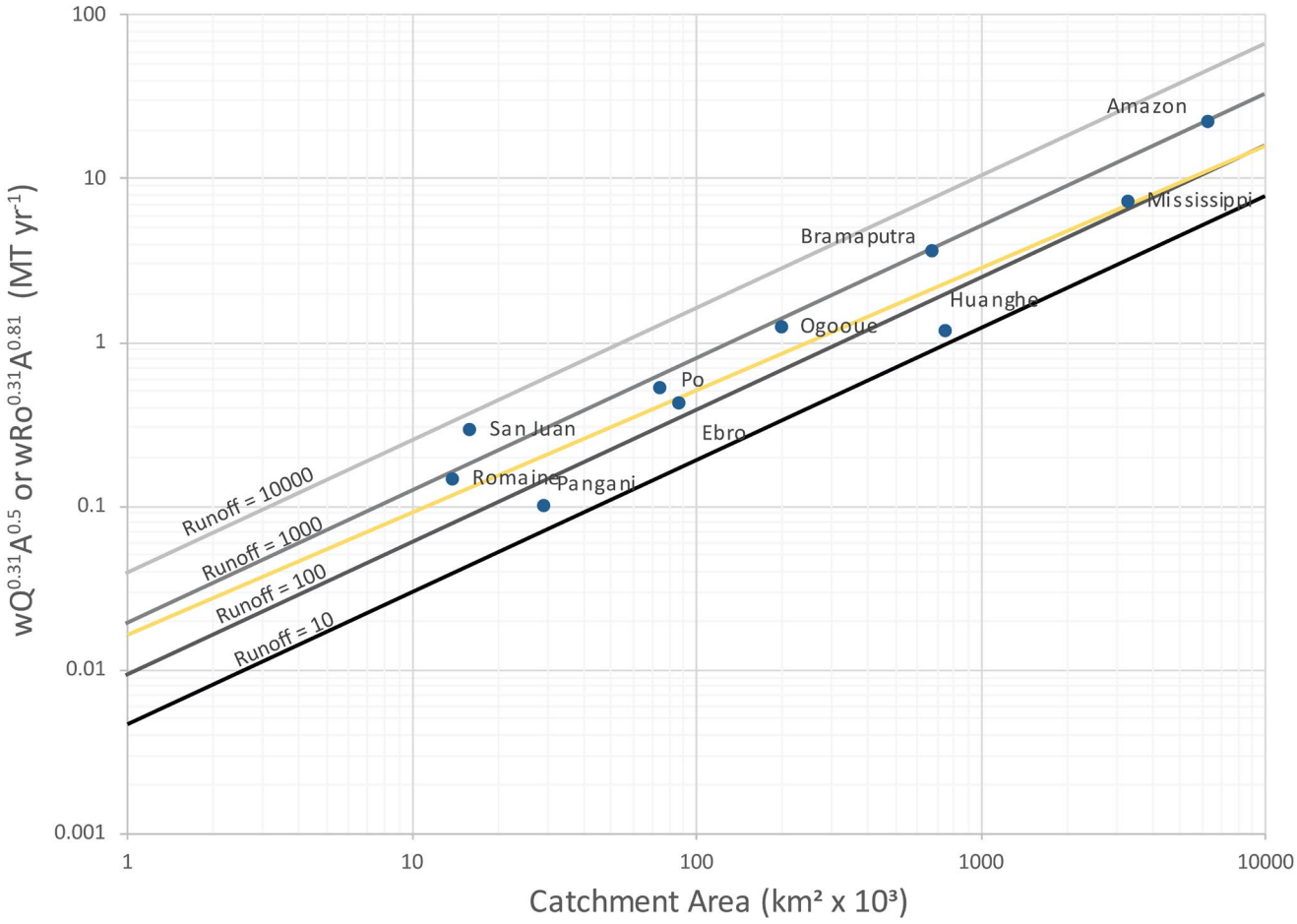

FIGURE 6 Correlation between influence of the functions w $Q^{0.31}A^{0.5}$ using improved water discharge calculation in Equation (5) or the simplified $wRo^{0.31}A^{0.81}$ equation against catchment area in explaining suspended sediment load (MT year^{-1}) for different run-off (*Ro*) rates from 10 to 10,000 mm/km year^{-1}. A selection of modern river catchments are overlain for reference. The yellow line shows the power-law relationship using the original water discharge parameter in Equation (4) by Syvitski and Milliman (2007). Catchment temperature (*T*), relief (*R*) and lithology (*B*) will scale linearly from the power-law relationship explained by either RoA or QA in the RoBART or BQART equations, respectively [Colour figure can be viewed at wileyonlinelibrary.com]

$wRo^{0.31}A^{0.81}$ in Figure 6. For example, if $wRo^{0.31}A^{0.81}$ explains 2 MT year^{-1} in Tss load and the combined values of parameters *B*, *R* and *T* equal 5 (e.g., 1 × 2.5 km × 2°C), then the resulting calculation on Tss load will yield 10 MT year^{-1}. The minimum and maximum combined constraints achieved in the *B*, *R* and *T* values will determine the accuracy of the resulting Tss load calculation. The *B* parameter shows a potential sixfold range based on the descriptions in Table 1 (0.5–3), however a twofold range may be appropriate for most systems (see Section 2.1). The maximum relief may vary by over 16-fold (0.5–8 km) based on modern river observations, although different tectonic regimes of varying system size will typically show a variability within sixfold (Figure 4).

Based on the global source-to-sink database of modern river catchments (Nyberg, Gawthorpe, et al., 2018), averaged annual catchment temperature in degree Celsius extend over an 18-fold range above the 2°C threshold (2–36°C). However, our understanding of the stratigraphic record and modelling of paleoclimates show that our confidence in estimating average annual catchment temperature is considerably better (e.g., ±4°C uncertainty in Sømme et al., 2013 or ±3°C in Brewer et al., 2020). Below the 2°C threshold, the *T* parameter is removed in Equation (6b) to derive the RoBAR formula, thus excluding the sensitivity of the parameter in the calculation of Tss load.

The sensitivity of the temperature parameter (*T*) on Tss load will thus differ based on whether the absolute temperature value is above or below 2°C. For example, if we assume a paleoclimate model can constrain temperature within a ±2°C range, then the uncertainty in the *T* parameter will impact predicted range in Tss load estimates to a greater degree for cooler climates (e.g., 6/2°C = 3-fold and 30/26°C = 1.15-fold variability). Figure 7 shows the average catchment temperature versus the sensitivity on the RoBART formula in calculating Tss load based on paleoclimate models with varying accuracy (i.e. ±2, 4 or 6°C). The RoBART model would suggest that as

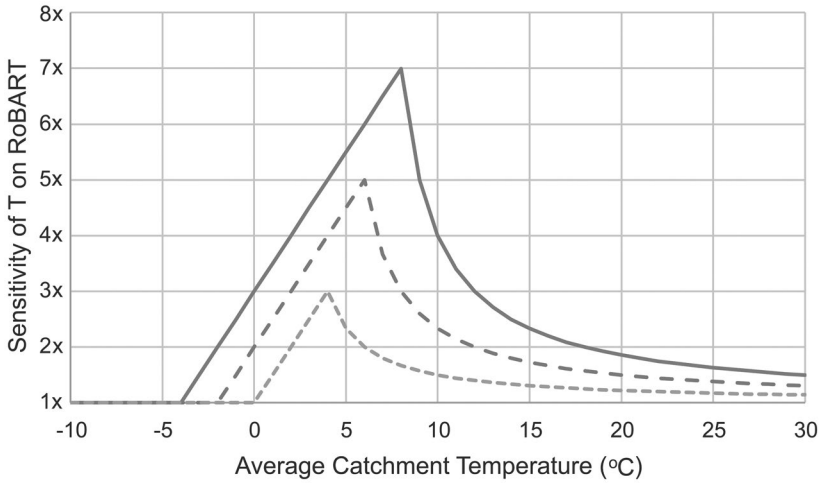

FIGURE 7 The sensitivity of the *T* parameter on the RoBART (and BQART) model based on different degrees of uncertainty around the modelled *T* parameter. Plotted against average catchment temperature, the results show a higher sensitivity on the RoBART model for colder climates

temperature decreases, uncertainty in predicting Tss load will increase to a peak until the lower *T* boundary reaches the 2°C threshold. Any *T* value below the 2°C threshold will be replaced by a value of 2 according to Equation (6b). Once both the lower and upper *T* parameter are below the 2°C threshold, temperature is not considered to influence the variability in calculating Tss load (e.g., 2/2 = 1-fold).

3.3 | Bedload material

In the reconstruction of a basin's infill history, it is important to consider both suspended and bedload material transport. In modern river systems, the global average of sediment transported as bedload material to the oceans is roughly estimated as 10% of the total sediment load (Curtis et al., 1973; Milliman & Meade, 1983). However, a large variability exists between different sediment routing systems with bedload material ranging significantly from <1% to over 90% of the total sediment load (Figure 8). The challenge is that bedload measurements are difficult and time consuming to gather with far less consistent long-term averaged empirical data than suspended sediment load (Turowski et al., 2010).

Current knowledge suggests that rivers with gravel-bed substrates such as the Fraser river, or large mud-substrate rivers around the equator like the Amazon river, have bedload transport rates representing less than 10% of its total sediment load (Babinski, 2005; Turowski et al., 2010). On contrary, the proportion of bedload transport in rivers with sand-rich substrates such as the Rhone (20%), Mississippi (33%), Ebro (40%), Ganges and Brahmaputra (51%) may be considerably higher (Figure 8). However, the controls on observed global bedload transport remain poorly understood with no correlations to, for instance, system size, relief, substrate erodibility or climate (Turowski et al., 2010).

It should be noted that the global-based compilation of bedload material transport in Figure 8 is based on the limited available data in literature. The dataset contains: (a) both sediment and transport limited systems (e.g., Amos et al., 2004; Kesel et al.,1992), (b) a variety of data collection methods (e.g., Vericat & Batalla, 2006; Lisimenka & Kubicki, 2019), and (c) measurements taken along different river reaches and flood stages (e.g., Antonelli et al., 2008; Cantalice et al., 2013). Nonetheless, in ancient S2S mass budget assessments, it is important to consider this uncertainty in estimating bedload material transport and the differences determined by gravel/mud versus sand-rich substrate fluvial environments.

3.4 | Monte Carlo simulations

To constrain predictions in Tss load based on the RoBART or BQART method, Monte Carlo simulations are often used to improve confidence in the practical bounds that define each parameter (e.g., Brewer et al., 2020; Sømme et al., 2013, 2019; Zhang et al., 2018). By applying probabilities that define the likelihood of a value to occur and randomly selecting a value from the population, a series of simulations (>10,000 iterations) can constrain the probable range in predicted sediment load.

Rectangular, triangular, log normal or normal as well as observed distributions from modern environments (e.g., (Zhang et al., 2018; Figure 4) may represent each parameter. The chosen distribution will depend on the constraints available within the study. A rectangular distribution for catchment area (*A*) and run-off (*Ro*) is common given its low and high estimate are equally as probable. A triangular or normal distribution for catchment lithology (*B*), relief (*R*) and temperature (*T*) is used to suggest a higher confidence in the mean/mode value (e.g., Brewer et al., 2020; Zhang et al., 2018). While there are six groups of lithologies in Table 1 defining a catchment's erodibility, those values represent an approximation (Cohen et al., 2013). Thus, the erodibility factor is a continuous value (Howard, 1994; Restrepo et al., 2015).

To show the sensitivity of Monte Carlo simulations on the RoBART (as well as BQART) equation, two hypothetical

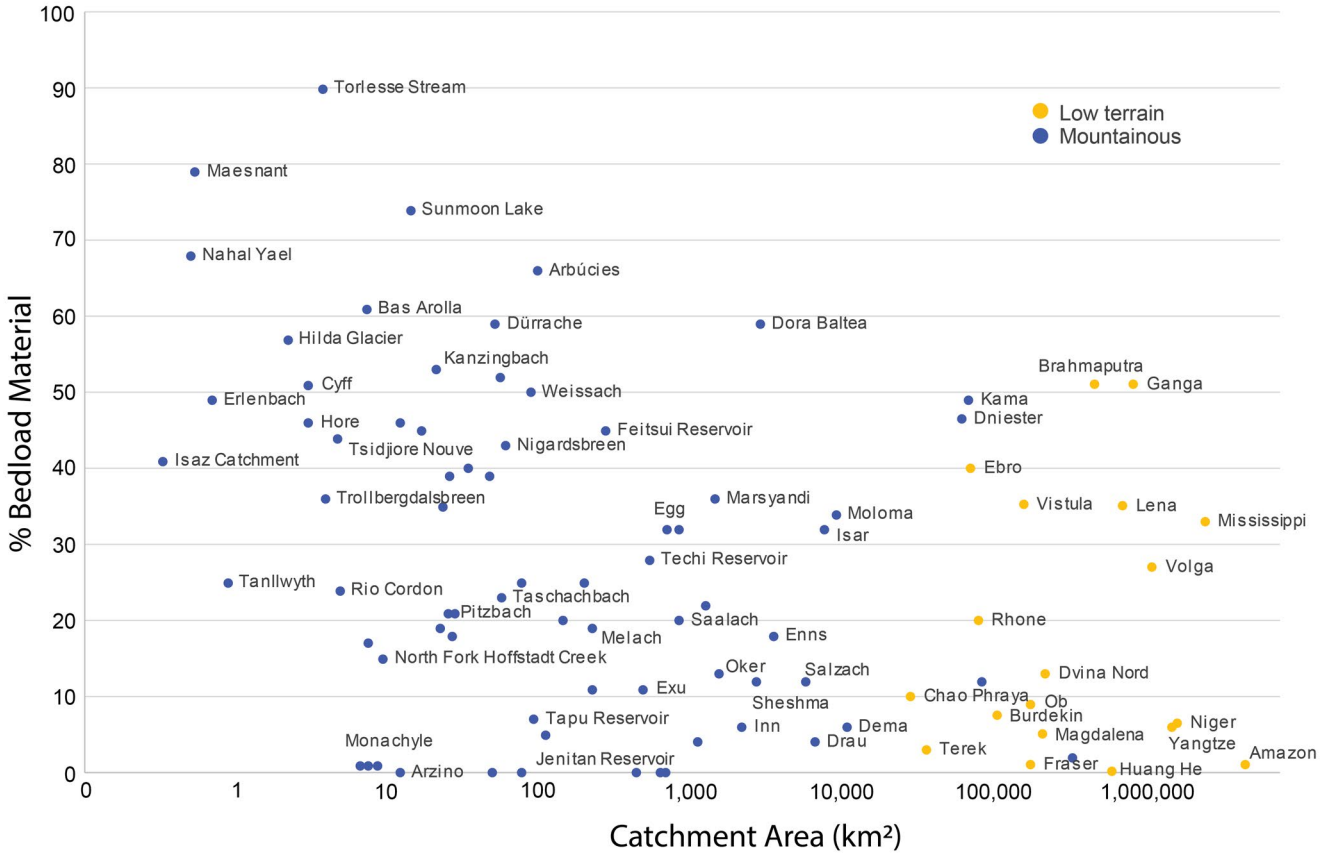

FIGURE 8 The proportion of a river's total sediment load as bedload material versus catchment area. Values are compiled for the pre-dam (if available) lowest available river reach conducted in each study. Dataset based on Smith (1986), Kesel et al. (1992), Antonelli et al. (2008), Vericat and Batalla (2006), Dada et al. (2018), Amos et al. (2004), Dunne et al. (1998), Babinski (2005), Cantalice et al. (2013), Turowski et al. (2010), Bidorn et al. (2015) and Lisimenka and Kubicki (2019). Blue and yellow points indicate if the sampled locations are within a mountainous or low-terrain region, respectfully, based on the distribution of modern sedimentary basins (Nyberg, Helland-Hansen, et al., 2018) [Colour figure can be viewed at wileyonlinelibrary.com]

scenarios are used to test a low and high range of uncertainty in the *B*, *R* and *T* values based on typical ranges constrained in previous studies (e.g., Brewer et al., 2020; Lyster et al., 2020; Sømme et al., 2013; Zhang et al., 2018). Low and high uncertainty in the *B* range were defined as twofold (1–2) and threefold (1–3), respectively (see previous discussion in Section 2.1). Low and high uncertainty in the *R* range were defined as twofold (2–4 km) and fivefold (1–5 km), respectively. Low and high uncertainty in the *T* range were defined as ±2 and ±4°C, respectively. A triangular distribution was created for each parameter with a mode equal to the mean of each range. For each run, 100,000 simulations were computed for every temperature step between −10 and 30°C. The sensitivity of *B*, *R* and *T* distributions on the RoBART equation were subsequently calculated as the ratio between the 90th and 10th percentile of each Tss distribution generated at every averaged catchment temperature step (Figure 9).

Each line in Figure 9 represents a different scenario based on a combination of either a low or high uncertainty in the *B*, *R* and *T* parameters. Each scenario has a given sensitivity on the RoBART formula that is shown on the left-hand axis (i.e. 2× equals twofold). To determine if a RoBART (or BQART) approach can derive an estimate of Tss load below one order of magnitude, the uncertainty in catchment area along the right-hand axis of Figure 9 should be cross-referenced to make sure it occurs above the chosen BRT scenario line for a given average catchment temperature. With increasing uncertainty in catchment area (*A*) down the right-hand axis, the reliability in *B*, *R* and *T* estimates will need to improve to maintain a one order of magnitude confidence in predicted Tss load. For example, given an averaged paleo-catchment temperature of 15°C and a high uncertainty in both *R* (1–5 km) and *T* (±4°C) (orange line; Figure 9), then the uncertainty in catchment area needs to be less than 4-fold (e.g., 100–400 km^2) to keep the range in Tss load estimates below one order of magnitude. [Correction added on 11 May 2021 after first publication. The final sentence in column two of this page has been edited for clarity at the request of the author.]

The overall trend in the Monte Carlo simulations shows that sensitivity of the *T* parameter towards colder climates remains prominent. A high uncertainty in the *T* parameter (±4°C) may impact the range in predicted Tss load by up to

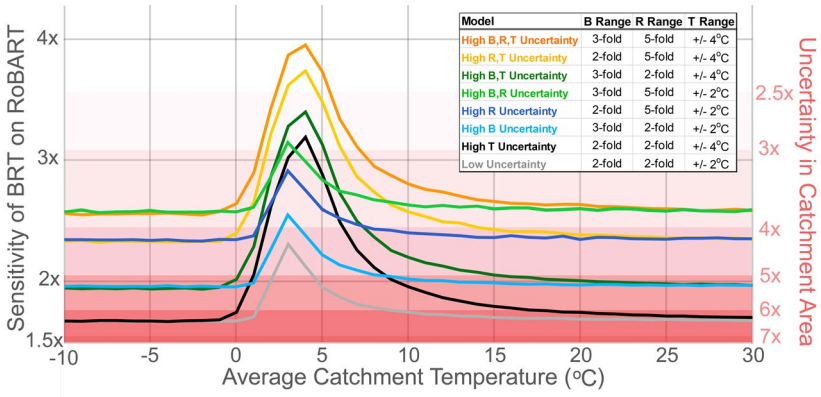

FIGURE 9 Shows the sensitivity of parameters BRT on the RoBART equation versus average catchment temperature for different scenarios using Monte Carlo simulations. The right-hand y axis and corresponding red color bars show the thresholds below which uncertainty in catchment area is needed to maintain an estimated Tss load calculation below one order of magnitude. For any given scenario and average catchment temperature, cross reference against the right-hand axis to determine uncertainty in catchment area for a given S2S study within the threshold. See main text for discussion [Colour figure can be viewed at wileyonlinelibrary.com]

50% compared to a low uncertainty in *B*, *R* and *T* model (gray line in Figure 9). However, as average catchment temperature decreases below 0°C or above 25°C, a high uncertainty in the *T* parameter (±4°C) will influence the range in predicted Tss load by less than 5%. A high uncertainty in relief or lithology will uniformly increase predicted range in Tss load estimates by as much as 40% and 17%, respectively. Combined high uncertainty in *B*, *R* and *T* show an increased range in predicted Tss load by as much as 70% compared to the low uncertainty model.

Figure 9 should be used as a quick point of reference to assess the applicability of the RoBART (or BQART) method for an ancient S2S study before investing time in Monte Carlo simulations. It should be noted that the figure includes a constant run-off range from 100 to 250 km^{-1} $year^{-1}$ corresponding to a conservative low estimate sensitivity on the RoBART formula of a semi-arid climate (see Section 3.2). The final distributions chosen for each parameter (rectangular, triangular, log normal or normal) for use in Monte Carlo simulations will ultimately determine the method's suitability. However, it is essential that each distribution chosen are geologically justified.

3.5 | A word on reconstructing catchment properties

If the purpose of a RoBART (or BQART) methodology is to reconstruct catchment properties based on time constrained observed sediment volume from the subsurface or outcrop, then RoBART may be reorganized to estimate relief and catchment area by:

$$R = \frac{Tss}{wRo^{0.31}BA^{0.81}T} \tag{7a}$$

$$A = \left(\frac{Tss}{wRo^{0.31}BRT}\right)^{1.235} \tag{7b}$$

A common reason for reconstructing a catchment property using the RoBART (or BQART) method is to better understand the landscape evolution of a region, as is the case for the poorly constrained topography of the Norwegian Jurassic-Paleocene hinterland (Sømme et al., 2013).

However, it is important that sediment rate estimates (volume / time) are representative only of Tss load and excludes or incorporates the uncertainty associated with bedload material transport (see Section 3.3). Furthermore, the estimated stratigraphic volume of Tss needs to contain a degree of uncertainty related to the accuracy of subsurface horizon mapping, depth conversion, density distributions in volume estimations, biostratigraphy accuracy, hiatuses, erosion and sediment bypass to name a few (cf. Guillocheau et al., 2012). In addition, the uncertainty in each parameter of the RoBART equation needed to solve for *R* or *A* should be considered. Reconstructing catchment properties using the RoBART (or BQART) thus contain significant sources of potential uncertainty that limit its applicability.

4 | DISCUSSION

The following section outlines a recommended workflow for RoBART (or BQART) mass budget S2S analysis. Furthermore, the limitations in the original empirical BQART method as well as considerations in extrapolating modern sediment load observations for ancient sedimentary systems will be discussed. Finally, the applicability of a BQART mass budget approach for different sedimentary

systems, time of investigation and boundary conditions are considered.

4.1 | Workflow

Based on the review of the practical bounds, sensitivity and uncertainty that define each parameter in the RoBART (or original BQART) method we recommend the following workflow for each studied paleogeography (Figure 10). The number of paleogeographic reconstructions in the broader analysis of a sedimentary system will depend on the change in boundary conditions (refer to limitations and applicability discussions in Sections 4.2 and 4.3).

4.1.1 | Suitability

Based on a first-pass analysis of the parameters in the RoBART model, determine the suitability of the approach for a particular non-glaciated S2S study. Published paleogeography and paleoclimate models can help to define a rough estimate for *A* and *T* parameters, and when applied to Figure 9, further determine the suitability of the method. It is recommended to apply the high uncertainty in temperature (±4°C) and relief (5-fold) as those parameters are typically the least constrained (Brewer et al., 2020; Lyster et al., 2020). If a first-pass analysis can further constrain *R*, *T* or *B* parameters, one of the other available trends in Figure 9 can be applied to determine the RoBART (or BQART) methods suitability in an ancient S2S mass budget assessment.

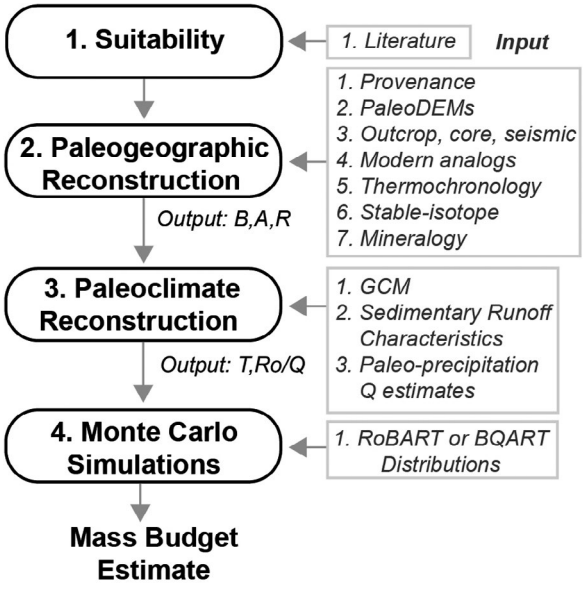

FIGURE 10 Recommended workflow to implement BQART (or RoBART) mass budget analyses for ancient source-to-sink systems

4.1.2 | Paleogeographic reconstruction (*B*, *A*, *R*)

Define the paleogeography of the study region using published reconstructions to define geometric and lithological attributes of parameters *B*, *A* and *R*. Seismic, outcrop and core data should supplement the study by constraining the likely river mouth locality that defines the drainage outlet. Available provenance and mineralogy studies (e.g., Blum et al., 2017; Dickinson, 1985; Dickinson & Gehrels, 2008; Ingersoll & Suczek, 1979) should further constrain both source region extent and lithology predictions in Table 1. Thermochronology (Reiners, 2007),stable-isotope based estimations (e.g. Rowley & Garzione, 2007) and modern analogues (e.g., Figure 4; Nyberg, Gawthorpe, et al., 2018; Sømme et al., 2009) will further help to refine results for catchment area and relief. If paleoDEM datasets area are available (e.g., Markwick & Valdes, 2004; Scotese & Wright, 2018), the delineation of catchments should strengthen the previous catchment area and relief estimates.

4.1.3 | Paleoclimate reconstruction (*T*, *Ro*)

If core or outcrop data are available, deduce the run-off characteristics that define either an arid, semi-arid, wet or humid climate as described by Eide, Müller, et al. (2018). Define the lower and upper range in run-off characteristics that describe each climate zone as stated in Table 2 and apply to Equation (5). General circulation models (GCM) can supplement the observed stratigraphy with use of paleoclimate modelling (e.g., Jacob et al., 2001; Markwick & Valdes, 2004; Sellwood & Valdes, 2008). Paleoclimate models should furthermore constrain the likely catchment averaged temperature (*T*) parameter. If precipitation estimates are available to define water discharge (*Q*), the value can directly be inserted into the original BQART model.

4.1.4 | Monte Carlo simulations

Monte Carlo simulations should be used to improve the uncertainty in predicted Tss load based on the ranges in expected *Ro*, *B*, *A*, *R* and *T* parameters. For parameters *B*, *R* and *T*, a geologically justified distribution should be considered given the parameters are based either on the non-explicit descriptions of lithology in Table 2 or based on models that contain a degree of confidence (*R* and *T*). Monte Carlo simulations may further be refined if geological evidence supports a distribution for the *Ro*/*Q* and *A* parameters. Apply a statistically significant number of iterations (typically >10,000) and extract the 10th and 90th percentile of the resulting Tss load predictions to define the likely low and high mass budget estimates.

4.2 | Limitations

One major limiting factor in the application of the BQART method for ancient S2S studies is that modern observations (ca. 30 year) do not capture the higher amplitude discharge events that may contribute a larger portion of sediments delivered to river mouths on deep geological time (Blum & Hattier-Womack, 2009; Helland-Hansen et al., 2016; Romans et al., 2016). The BQART method was not designed to explain the dynamic relationship observed between water discharge and sediment supply from climate fluctuations on a 10^2–10^6 year timescale or the differences in supply limited versus transport limited systems (Romans et al., 2016). For example, smaller catchments may be more sensitive to the higher water discharge events with shorter transfer zones from hinterland to ocean compared to larger sediment routing systems (e.g., Nyberg, Helland-Hansen, et al., 2018; Warrick & Milliman, 2003). In fact, the true impact of sediment signal propagation and shredding on the marine stratigraphic record are still aspects of ongoing debate and research (Blum & Hattier-Womack, 2009; Helland-Hansen et al., 2016; Jerolmack & Paola, 2010; Nyberg, Helland-Hansen, et al., 2018; Romans et al., 2016).

It is furthermore important to recognize that the BQART (and RoBART) method is not a morphodynamic landscape evolution model (e.g., Braun & Willett, 2013) that considers a changing topography over time, rather a method to estimate mass-budget over discrete time-intervals. Smaller tectonically active sedimentary basins such as strike-slip, extensional and fore-arc settings with a basin lifespan on the order of ca. 10 Myr (Ingersoll, 2011; Nyberg & Howell, 2015) may experience rapidly changing catchment morphology and sediment load (Nyberg, Helland-Hansen, et al., 2018). On the other hand, larger foreland and passive margins with a basin lifespan in the order of ca. 100 Myr (Ingersoll, 2011; Nyberg & Howell, 2015) are less likely to experience as rapid changes in catchment morphology and sediment load compared to smaller, active systems (Nyberg, Helland-Hansen, et al., 2018). It is therefore important to determine the number of paleogeographic reconstructions in a S2S study according to the recurrence time of major paleogeographic shifts for a BQART (or RoBART) mass budget estimate.

It is also important to reiterate that bedload material transport is not considered in a BQART approach resulting in an underestimated total sediment load calculation (Lyster et al., 2020). As shown in Figure 8, the impact of bedload material transport on the total sediment load budget can be significant though remains poorly understood (Turowski et al., 2010). In addition, the BQART method does not explain intra-catchment variability and was built to show decadal-term (ca. 30 years) averaged total suspended sediment load where rivers enter the ocean (Figure 1; Syvitski & Milliman, 2007). However, recent numerical implementation of the BQART equation have shown its applicability in modelling suspended sediment load of the continental United States, based on the limited available gauging stations in upstream river reaches (Cohen et al., 2013).

Finally, while BQART accounts for increased and decreased sediment load from human landuse change and damming within the *B* parameter, humans have cultivated livelihoods near river systems and floodplains before any record of river systems behaviour. For instance, Milliman and Syvitski (1992) suggest that deforestation and farming 2000–2500 years ago may have increased natural sediment loads by twofold. On the other hand, most of the world's rivers are influenced by the regulation of water flow and the trapping of sediments behind dams (Grill et al., 2019; Vörösmarty et al., 2003). In other words, the BQART equation may either under- or over-estimate sediment load of a sedimentary system by comparing observed sediment load at gauging stations with an unknown pristine environment. The uncertainty on the impact of early human landuse in establishing a pristine empirical model of sediment load will propagate in its application to the ancient and hence, it is crucial, if only modest, to include a degree of variance around the *B* parameter for a catchment's erodibility factor.

4.3 | Applicability

The practical bounds that define each parameter in the BQART model show that catchment area and relief are the least constrained in comparison to lithology, water discharge and temperature (Brewer et al., 2020). Yet the sensitivity of each parameter indicates the reliability in the model will also vary by a catchment's average temperature (Figure 9). Based on the practical bounds and sensitivity that define each parameter, as well as the limitations highlighted above, the applicability of the BQART method for non-glacial S2S systems (see Section 2.1) is suggested to depend on the time of investigation, uncertainty in each parameter and climate conditions.

For deep-time investigation (> ca. 10^7 years) the method is most applicable to large (>10,000 km^2) exorheic S2S systems on a regional and continental scale of cold (<2°C) or warm temperate (>8°C) climates. Given constraints on catchment area and relief are less reliable for deep geological time where landscapes are not preserved (Brewer et al., 2020; Helland-Hansen et al., 2016), the uncertainty and sensitivity of the temperature parameter becomes crucial in assessing the applicability of BQART (Figures 7 and 9). Larger less tectonically active sedimentary systems (e.g., foreland, passive margins) are therefore also more appropriate for a deep-time investigation and predictions may be run on the order of 10^6 years. However, sub-orbital and orbital climate fluctuations operating on timescales of 10^2 to 10^6 years (Romans

et al., 2016), not captured in the modern BQART method, will be a source of uncertainty. Despite these shortcomings, Zhang et al., 2018; Lyster et al. (2020); Brewer et al. (2020) and others note that well-constrained paleogeographic reconstructions of warm temperate systems can achieve BQART Tss load estimates to within one order of magnitude in observed sediment volume.

For application to intermediate-time investigations (< ca. 10^7 year), improved constraints on catchment area and relief parameters will improve confidence in predicted Tss load estimates. Watkins et al. (2018) show for instance that BQART estimates of Tss load performed well-compared to mapped offshore sediment volumes of the Holocene in the Gulf of Corinth, Greece. Despite a cooler climate (5–17°C) and smaller catchments (>5 km^2), the authors higher confidence in the Holocene catchment area and relief produces reasonable mass budget estimates. The shorter timestep predictions used in mass budgets estimates (ca. 10^5 year) constrained by detailed paleogeographic maps can be applied to smaller tectonically active sedimentary basins (e.g., forearc, extensional, strike-slip). However, temperature sensitivity and higher discharge events due to climatic fluctuations are a large potential source of uncertainty for these basins. In general, though, less tectonically active sediment routing systems (e.g., foreland, passive margins) will remain the most reliable in BQART mass budget assessments.

Ultimately, the range in predicted Tss load estimates and thus applicability of BQART will depend on the uncertainty and sensitivity related to each parameter and timescale for predictions that will vary on a case-by-case basis.

5 | CONCLUSIONS

In this study we have explored the practical bounds, uncertainty and sensitivity that define the BQART parameters and discussed the practicality in its applicability to ancient S2S studies. In conclusion, the study has found:

1. The RoBART (or BQART) method is most suitable for large regional to continental scale S2S systems of cold (<2°C) or warm temperate (>8°C) sedimentary systems. In application to deep time systems (>10^6), higher uncertainty in catchment area and relief will mean that constraining the temperature parameter is crucial for its applicability. A framework has been developed to assess the applicability of the RoBART method based on the catchments average temperature (T) and a low or high uncertainty in range of B, R and T in relation to catchment size predictions.
2. A limiting factor in applying modern observations of sediment load to predict ancient mass budgets is a lack of consideration to the high discharge events that may dominate the stratigraphic record. Furthermore, our understanding of bedload transport and its relation to the total sediment budget both in the modern and in a long-term source-to-sink perspective is lacking. It is therefore important for mass budget approaches based on empirical data to consider the uncertainty related to both high discharge events and bedload material transport.
3. Improved water discharge estimates may simplify the BQART model analytically to create the RoBART equation. By implementing more realistic water discharge scaling, prediction in Tss load estimates improves significantly. Over 83% of river catchments are explained within a 2-fold range to observations in the RoBART method compared to 69% in the original BQART method. Constrains on water discharge and its power-law scaling relationship suggests that the parameter is the least sensitive in estimating Tss load.
4. Estimates of catchment area and relief are generally the least constrained. The sensitivity of catchment area on predicted Tss load scales by a power-law relationship and is thus less sensitive than relief on the RoBART (or BQART) method yet spans five orders in magnitude. Relief constraints are typically within a sixfold range based on modern observations of river catchments, but scale linearly in the RoBART equation. Thus, uncertainty in catchment area and/or relief can have a significant impact on predicted Tss load.
5. Average catchment temperature (T) can reasonably be constrained based on paleoclimate modelling. However, the sensitivity of the parameter on the RoBART (or BQART) model will depend on the absolute temperature. In Monte Carlo simulations, cooler climates (2°C–8°C) can increase the uncertainty in predicted Tss load by as much as 50% compared to less than 5% for cold (<0°C) or warm (>25°C) climates.

ACKNOWLEDGEMENTS

The authors thank Gavin Elliott, Alex Whittaker and Glenn Sharman in addition to editor Cari Johnson for giving constructive feedback and comments that strengthened the manuscript. The project was funded under the Spatial-Temporal Reconstruction of Basin Fills project (no. 810127) by Equinor. Gawthorpe acknowledges the VISTA Professor award from The Norwegian Academy of Science and Letters.

CONFLICT OF INTEREST

The authors do not declare any conflict of interest.

PEER REVIEW

The peer review history for this article is available at https://publons.com/publon/10.1111/bre.12563.

DATA AVAILABILITY STATEMENT

The datasets used in this study are freely accessible including the global modern river observations of Milliman and Farnsworth (2011) and the M&S92+ database in Syvitski and Milliman (2007). The Global Source to Sink database in Nyberg, Helland-Hansen, et al. (2018) is available at https://dataverse.harvard.edu/dataset.xhtml?persistentId=doi:10.7910/DVN/ETH8VN. Python scripts for the Monte Carlo simulations are available upon request.

ORCID

Björn Nyberg https://orcid.org/0000-0002-4910-2417
William Helland-Hansen https://orcid.org/0000-0002-7529-1485
Robert Gawthorpe https://orcid.org/0000-0002-4352-6366

REFERENCES

Allen, P. A., Armitage, J. J., Carter, A., Duller, R. A., Michael, N. A., Sinclair, H. D., Whitchurch, A. L., & Whittaker, A. C. (2013). The Qs problem: Sediment volumetric balance of proximal foreland basin systems. *Sedimentology*, *60*, 102–130. https://doi.org/10.1111/sed.12015

Amos, K. J., Alexander, J., Horn, A., Pocock, G. D., & Fielding, C. R. (2004). Supply limited sediment transport in a high-discharge event of the tropical Burdekin River, North Queensland, Australia. *Sedimentology*, *51*, 145–162. https://doi.org/10.1111/j.1365-3091.2004.00616.x

Antonelli, C., Eyrolle, F., Rolland, B., Provansal, M., & Sabatier, F. (2008). Suspended sediment and 137Cs fluxes during the exceptional December 2003 flood in the Rhone River, southeast France. *Geomorphology*, *95*, 350–360. https://doi.org/10.1016/j.geomorph.2007.06.007

Armstrong, H. A., Wagner, T., Herringshaw, L. G., Farnsworth, A. J., Lunt, D. J., Harland, M., & Atar, E. F. L. (2016). Hadley circulation and precipitation changes controlling black shale deposition in the Late Jurassic Boreal Seaway. *Paleoceanography*, *31*(8), 1041–1053. https://doi.org/10.1002/2015PA002911

Babinski, Z. (2005). *The relationship between suspended and bed load transport in river channels*. Sediment budgets. Proceedings of symposium S1 held during the Seventh IAHS Scientific Assembly at Foz do Iguaçu, Brazil, April 2005. IAHS Publ. 291, 2005.

Bhattacharya, J. P., Copeland, P., Lawton, T. F., & Holbrook, J. (2016). Estimation of source area, river paleo-discharge, paleoslope, and sediment budgets of linked deep-time depositional systems and implications for hydrocarbon potential. *Earth-Science Reviews*, *153*, 77–110. https://doi.org/10.1016/j.earscirev.2015.10.013

Bidorn, B., Chanyotha, S., Kish, S. A., Donoghue, J. F., Bidorn, K., & Mama, R. (2015). The effects of Thailand's Great Flood of 2011 on river sediment discharge in the upper Chao Phraya River basin, Thailand. *International Journal of Sediment Research*, *30*, 328–337. https://doi.org/10.1016/j.ijsrc.2015.10.001

Blum, M. D., & Hattier-Womack, J. (2009). Climate change, sea-level change, and fluvial sediment supply to deepwater depositional systems. In B. Kneller, O. J. Martinsen, & B. McCaffrey (Eds.), *External controls on deep-water depositional systems* (pp. 15–39). SEPM, Special Publication. https://doi.org/10.2110/sepmsp.092.015

Blum, M. D., Milliken, K. T., Pecha, M. A., Snedden, J. W., Frederick, B. C., & Galloway, W. E. (2017). Detrital-zircon records of Cenomanian, Paleocene, and Oligocene Gulf of Mexico drainage integration and sediment routing: Implications for scales of basin-floor fans. *Geosphere*, *13*(6), 2169–2205. https://doi.org/10.1130/GES01410.1

Braun, J., & Willett, S. D. (2013). A very efficient O(n), implicit and parallel method to solve the stream power equation governing fluvial incision and landscape evolution. *Geomorphology*, *180–181*, 170–179. https://doi.org/10.1016/j.geomorph.2012.10.008

Brewer, C. J., Hampson, G. J., Whittaker, A. C., Roberts, G. G., & Watkins, S. E. (2020). Comparison of methods to estimate sediment flux in ancient sediment routing systems. *Earth-Science Reviews*, *207*, 103217. https://doi.org/10.1016/j.earscirev.2020.103217

Cantalice, J. R. B., Cunha Filho, M., Stosic, B. D., Piscoya, V. C., Guerra, S. M. S., & Singh, V. P. (2013). Relationship between bed-load and suspended sediment in the sand-bed Exu River, in the semi-arid region of Brazil. *Hydrological Sciences Journal*, *58*, 1789–1802. https://doi.org/10.1080/02626667.2013.839875

Cohen, S., Kettner, A. J., Syvitski, J. P. M., & Fekete, B. M. (2013). WBMsed, a distributed global-scale riverine sediment flux model: Model description and validation. *Computers and Geosciences*, *53*, 80–93. https://doi.org/10.1016/j.cageo.2011.08.011

Cook, S. J., Swift, D. A., Kirkbride, M. P., Knight, P. G., & Waller, R. I. (2020). The empirical basis for modelling glacial erosion rates. *Nature Communications*, *11*(1), 1–7. https://doi.org/10.1038/s41467-020-14583-8

Covault, J. A., Craddock, W. H., Romans, B. W., Fildani, A., & Gosai, M. (2013). Spatial and temporal variations in landscape evolution: Historic and longer-term sediment flux through global catchments. *The Journal of Geology*, *121*, 35–56. https://doi.org/10.1086/668680

Curtis, W. F., Culbertson, J. K., & Chase, E. B. (1973). Fluvial-sediment discharge to the oceans from the conterminous United States. *US Geological Survey*, *670*, 17.

Dada, O. A., Li, G., Qiao, L., Asiwaju-Bello, Y. A., & Anifowose, A. Y. B. (2018). Recent Niger Delta shoreline response to Niger River hydrology: Conflict between forces of Nature and Humans. *Journal of African Earth Sciences*, *139*, 222–231. https://doi.org/10.1016/j.jafrearsci.2017.12.023

Dickinson, W. R. (1985). Interpreting provenance relations from detrital modes of sandstones. In G. Zuffa (Ed.), *Provenance of arenites. NATO ASI Series (Series C: Mathematical and Physical Sciences)* (pp. *148*, 333–361). Dordrecht: Springer.

Dickinson, W. R., & Gehrels, G. E. (2008). U-Pb ages of detrital zircons in relation to paleogeography: Triassic paleodrainage networks and sediment dispersal across southwest laurentia. *Journal of Sedimentary Research*, *78*(12), 745–764. https://doi.org/10.2110/jsr.2008.088

Dunne, T., Mertes, L. A. K., Meade, R. H., Richey, J. E., & Forsberg, B. R. (1998). Exchanges of sediment between the flood plain and channel of the Amazon River in Brazil. *Bulletin of the Geological Society of America*, *110*, 450–467.

Dürr, H. H., Meybeck, M., & Dürr, S. H. (2005). Lithologic composition of the Earth's continental surfaces derived from a new digital map emphasizing riverine material transfer. *Global Biogeochemical Cycles*, *19*(4). https://doi.org/10.1029/2005GB002515

Eide, C. H., Klausen, T. G., Katkov, D., Suslova, A. A., & Helland-Hansen, W. (2018). Linking an Early Triassic delta to antecedent topography: Source-to-sink study of the southwestern Barents Sea

margin. *Bulletin of the Geological Society of America*, *130*, 263–283. https://doi.org/10.1130/B31639.1

Eide, C. H., Müller, R., & Helland-Hansen, W. (2018). Using climate to relate water discharge and area in modern and ancient catchments. *Sedimentology*, *65*, 1378–1389. https://doi.org/10.1111/sed.12426

Gibling, M. R., & Davies, N. S. (2012). Palaeozoic landscapes shaped by plant evolution. *Nature Geoscience*, *5*, 99. https://doi.org/10.1038/ngeo1376

Grill, G., Lehner, B., Thieme, M., Geenen, B., Tickner, D., Antonelli, F., Babu, S., Borrelli, P., Cheng, L., Crochetiere, H., Ehalt Macedo, H., Filgueiras, R., Goichot, M., Higgins, J., Hogan, Z., Lip, B., McClain, M. E., Meng, J., Mulligan, M., … Zarfl, C. (2019). Mapping the world's free-flowing rivers. *Nature*, *569*(7755), 215–221. https://doi.org/10.1038/s41586-019-1111-9

Guillocheau, F., Rouby, D., Robin, C., Helm, C., Rolland, N., Carlier, L. E., de Veslud, C., & Braun, J. (2012). Quantification and causes of the terrigeneous sediment budget at the scale of a continental margin: A new method applied to the Namibia-South Africa margin. *Basin Research*, *24*, 3–30.

Hack, J. T. (1957). Studies of longitudinal profiles in Virginia and Maryland. *United States Geological Survey Professional Paper*, *294-B*, 1.

Helland-Hansen, W., Sømme, T. O., Martinsen, O. J., Lunt, I., & Thurmond, J. (2016). Deciphering earth's natural hourglasses: Perspectives on source-to-sink analysis. *Journal of Sedimentary Research*, *86*, 1008–1033. https://doi.org/10.2110/jsr.2016.56

Holbrook, J., & Wanas, H. (2014). A Fulcrum approach to assessing source-to-sink mass balance using channel paleohydrologic paramaters derivable from common fluvial data sets with an example from the cretaceous of Egypt. *Journal of Sedimentary Research*, *84*(5), 349–372. https://doi.org/10.2110/jsr.2014.29

Hovius, N. (1996). Regular spacing of drainage outlets from linear mountain belts. *Basin Research*, *8*, 29–44. https://doi.org/10.1111/j.1365-2117.1996.tb00113.x

Howard, A. D. (1994). A detachment-limited model of drainage basin evolution. *Water Resources Research*, *30*(7), 2261–2285. https://doi.org/10.1029/94WR00757

Ingersoll, R. V. (2011). Tectonics of sedimentary basins, with revised nomenclature. In C. Busby & A. Azor (Eds.), *Tectonics of sedimentary basins: Recent advances* (Firsted., pp. 1–43). Oxford: Blackwell Publishing Ltd. https://doi.org/10.1002/9781444347166.ch1

Ingersoll, R. V., & Suczek, C. A. (1979). Petrology and provenance of Neogene sand from Nicobar and Bengal fans, DSDP sites 211 and 218. *Journal of Sedimentary Research*, *49*(4), 1217–1228.

Jacob, R., Schafer, C., Foster, I., Tobis, M., & Anderson, J. (2001). Computational design and performance of the Fast Ocean Atmosphere Model, version one. Computational Science—ICCS 2001. In V. N. Alexandrov et al (Eds.), *Lecture Notes in Computer Science Series*, *2073*, 175–184.

Jerolmack, D. J., & Paola, C. (2010). Shredding of environmental signals by sediment transport. *Geophysical Research Letters*, *37*, Article L19401.

Kesel, R. H., Yodis, E. G., & McCraw, D. J. (1992). An approximation of the sediment budget of the lower Mississippi River prior to major human modification. *Earth Surface Processes and Landforms*, *17*, 711–722. https://doi.org/10.1002/esp.3290170707

Lin, C., Liu, S., Zhuang, Q., & Steel, R. J. (2018). Sedimentation of Jurassic fan-delta wedges in the Xiahuayuan basin reflecting thrust-fault movements of the western Yanshan fold-and-thrust belt, China. *Sedimentary Geology*, *368*, 24–43. https://doi.org/10.1016/j.sedgeo.2018.03.005

Lisimenka, A., & Kubicki, A. (2019). Bedload transport in the Vistula River mouth derived from dune migration rates, southern Baltic Sea. *Oceanologia*, *61*, 384–394. https://doi.org/10.1016/j.oceano.2019.02.003

Liu, Q., Zhu, X., Zeng, H., & Li, S. (2019). Source-to-sink analysis in an Eocene rifted lacustrine basin margin of western Shaleitian Uplift area, offshore Bohai Bay Basin, eastern China. *Marine and Petroleum Geology*, *107*, 41–58. https://doi.org/10.1016/j.marpetgeo.2019.05.013

Lyster, S. J., Whittaker, A. C., Allison, P. A., Lunt, D. J., & Farnsworth, A. (2020). Predicting sediment discharges and erosion rates in deep time—Examples from the late Cretaceous North American continent. *Basin Research*, *32*(6), 1547–1573. https://doi.org/10.1111/bre.12442

Markwick, P. J., & Valdes, P. J. (2004). Palaeo-digital elevation models for use as boundary conditions in coupled ocean–atmosphere GCM experiments: A Maastrichtian (late Cretaceous) example. *Palaeogeography, Palaeoclimatology, Palaeoecology*, *213*, 37–63. https://doi.org/10.1016/j.palaeo.2004.06.015

Milliman, J. D., & Farnsworth, K. L. (2011). *River discharge to the coastal ocean: A global synthesis*. Cambridge, UK: Cambridge University Press. https://doi.org/10.1017/CBO9780511781247

Milliman, J. D., & Meade, R. H. (1983). World-wide delivery of river sediment to the oceans. *Journal of Geology*, *91*, 1–21. https://doi.org/10.1086/62874110.1086/628741

Milliman, J. D., & Syvitski, J. P. M. (1992). Geomorphic/tectonic control of sediment discharge to the ocean: The importance of small mountainous rivers. *The Journal of Geology*, *100*, 525–544. https://doi.org/10.1086/629606

Nyberg, B., Gawthorpe, R. L., & Helland-hansen, W. (2018). Geomorphology The distribution of rivers to terrestrial sinks: Implications for sediment routing systems. *Geomorphology*, *316*, 1–23. https://doi.org/10.1016/j.geomorph.2018.05.007

Nyberg, B., Helland-Hansen, W., Gawthorpe, R. L., Sandbakken, P., Eide, C. H., Sømme, T., & Leiknes, S. (2018). Revisiting morphological relationships of modern source-to-sink segments as a first-order approach to scale ancient sedimentary systems. *Sedimentary Geology*, *373*, 111–133. https://doi.org/10.1016/j.sedgeo.2018.06.007

Nyberg, B., & Howell, J. A. (2015). Is the present the key to the past? A global characterization of modern sedimentary basins. *Geology*, *43*(7), 643–646. https://doi.org/10.1130/G36669.1

Petter, A. L., Steel, R. J., Mohrig, D., Kim, W., & Carvajal, C. (2013). Estimation of the paleoflux of terrestrial-derived solids across ancient basin margins using the stratigraphic record. *GSA Bulletin*, *125*(3–4), 578–593. https://doi.org/10.1130/B30603.1

Reiners, P. W. (2007). Thermochronologic approaches to paleotopography. *Reviews in Mineralogy and Geochemistry*, *66*(1), 243–267. https://doi.org/10.2138/rmg.2007.66.10

Restrepo, J. D., Kettner, A. J., & Syvitski, J. P. M. (2015). Recent deforestation causes rapid increase in river sediment load in the Colombian Andes. *Anthropocene*, *10*, 13–28. https://doi.org/10.1016/j.ancene.2015.09.001

Rigon, R., Rodriguez-Iturbe, I., Maritan, A., Giacometti, A., Tarboton, D. G., & Rinaldo, A. (1996). On Hack's Law. *Water Resources Research*, *32*(11), 3367–3374. https://doi.org/10.1029/96WR02397

Romans, B. W., Castelltort, S., Covault, J. A., Fildani, A., & Walsh, J. P. (2016). Environmental signal propagation in sedimentary systems

across timescales. *Earth-Science Reviews*, *153*, 7–29. https://doi.org/10.1016/j.earscirev.2015.07.012

Rowley, D. B., & Garzione, C. N. (2007). Stable isotope-based paleoaltimetry. *Annual Review of Earth and Planetary Sciences*, *35*(1), 463–508. https://doi.org/10.1146/annurev.earth.35.031306.140155

Scotese, C. R., & Wright, N. (2018). PALEOMAP paleodigital elevation models (PaleoDEMS) for the phanerozoic. https://www.earthbyte.org/paleodem-resource-scotese-and-wright-2018/

Sellwood, B., & Valdes, P. (2008). Jurassic climates. *Proceedings of the Geologists' Association*, *119*, 5–17. https://doi.org/10.1016/S0016-7878(59)80068-7

Smith, D. G. (1986). Anastomosing river deposits, sedimentation rates and basin subsidence, Magdalena River, northwestern Colombia, South America. *Sedimentary Geology*, *46*, 177–196. https://doi.org/10.1016/0037-0738(86)90058-8

Sømme, T. O., Helland-hansen, W., Martinsen, O. J., & Thurmond, J. B. (2009). Relationships between morphological and sedimentological parameters in source-to-sink systems: A basis for predicting semi-quantitative characteristics in subsurface systems. *Basin Research*, *21*, 361–387. https://doi.org/10.1111/j.1365-2117.2009.00397.x

Sømme, T. O., Martinsen, O. J., & Lunt, I. (2013). Linking offshore stratigraphy to onshore paleotopography: The Late Jurassic-Paleocene evolution of the south Norwegian margin. *Bulletin of the Geological Society of America*, *125*, 1164–1186. https://doi.org/10.1130/B30747.1

Somme, T. O., Piper, D. J. W., Deptuck, M. E., & Helland-Hansen, W. (2011). Linking onshore-offshore sediment dispersal in the golo source-to-sink system (Corsica, France) during the late quaternary. *Journal of Sedimentary Research*, *81*(2), 118–137. https://doi.org/10.2110/jsr.2011.11

Sømme, T. O., Skogseid, J., Embry, P., & Løseth, H. (2019). Manifestation of tectonic and climatic perturbations in deep-time stratigraphy—An example from the paleocene succession offshore Western Norway. *Frontiers in Earth Science*, *7*, 303. https://doi.org/10.3389/feart.2019.00303

Syvitski, J. P. M., & Milliman, J. D. (2007). Geology, geography, and humans battle for dominance over the delivery of fluvial sediment to the coastal ocean. *The Journal of Geology*, *115*(1), 1–19. https://doi.org/10.1086/509246

Turowski, J. M., Rickenmann, D., & Dadson, S. J. (2010). The partitioning of the total sediment load of a river into suspended load and bedload: A review of empirical data. *Sedimentology*, *57*, 1126–1146. https://doi.org/10.1111/j.1365-3091.2009.01140.x

Vericat, D., & Batalla, R. J. (2006). Sediment transport in a large impounded river: The lower Ebro, NE Iberian Peninsula. *Geomorphology*, *79*, 72–92. https://doi.org/10.1016/j.geomorph.2005.09.017

von Blanckenburg, F. (2005). The control mechanisms of erosion and weathering at basin scale from cosmogenic nuclides in river sediment. *Earth and Planetary Science Letters*, *237*, 462–479. https://doi.org/10.1016/j.epsl.2005.06.030

Vörösmarty, C. J., Meybeck, M., Fekete, B., Sharma, K., Green, P., & Syvitski, J. P. M. (2003). Anthropogenic sediment retention: Major global impact from registered river impoundments. *Global and Planetary Change*, *39*(1), 169–190. https://doi.org/10.1016/S0921-8181(03)00023-

Warrick, J. A., & Milliman, J. D. (2003). Hyperpycnal sediment discharge from semiarid southern California rivers: Implications for coastal sediment budgets. *Geology*, *31*, 781–784. https://doi.org/10.1130/G19671.1

Watkins, S. E., Whittaker, A. C., Bell, R. E., McNeill, L. C., Gawthorpe, R. L., Brooke, S. A. S., & Nixon, C. W. (2019). Are landscapes buffered to high-frequency climate change? A comparison of sediment fluxes and depositional volumes in the Corinth Rift, central Greece, over the past 130 k.y. *GSA Bulletin*, *131*(3-4), 372–388. https://doi.org/10.1130/B31953.1

Zhang, J., Covault, J., Pyrcz, M., Sharman, G., Carvajal, C., & Milliken, K. (2018). Quantifying sediment supply to continental margins: Application to the Paleogene Wilcox Group, Gulf of Mexico. *AAPG Bulletin*, *102*(9), 1685–1702. https://doi.org/10.1306/01081817308

How to cite this article: Nyberg B, Helland-Hansen W, Gawthorpe R, Tillmans F, Sandbakken P. Assessing first-order BQART estimates for ancient source-to-sink mass budget calculations. *Basin Res*. 2021;33:2435–2452. https://doi.org/10.1111/bre.12563